

1 **A conceptual model-based sediment connectivity assessment for patchy agricultural catchments**

2 Pedro V. G. Batista<sup>1\*</sup>, Peter Fiener<sup>2</sup>, Simon Scheper<sup>1,3</sup>, Christine Alewell<sup>1</sup>

3 <sup>1</sup>Department of Environmental Sciences, Universität Basel, Bernoullistrasse 30, 4056, Basel,  
4 Switzerland.

5 <sup>2</sup>Institute for Geography, Universität Augsburg, Alter Postweg 118, 86159, Augsburg, Germany.

6 <sup>3</sup>Dr. Simon Scheper – Research | Consulting | Teaching, Eickhorst 3, 29413 Dähre, Germany

7

8 \*pedro.batista@unibas.ch

9

10 **Abstract**

11 The accelerated sediment supply from agricultural soils to riverine and lacustrine environments leads  
12 to negative off-site consequences. In particular, the sediment connectivity from agricultural land to  
13 surface waters is strongly affected by landscape patchiness and the linear structures that separate field  
14 parcels (e.g. roads, tracks, hedges, and grass buffer strips). Understanding the feedbacks between these  
15 structures and sediment transfer is therefore crucial for minimising off-site erosion impacts. Although  
16 soil erosion models can be used to understand lateral sediment transport patterns, model-based  
17 connectivity assessments are hindered by the uncertainty in model structures and input data. In  
18 particular, the representation of linear landscape features in numerical soil redistribution models is  
19 often compromised by the spatial resolution of the input data and the quality of the process  
20 descriptions. Here we adapted the WaTEM/SEDEM model using high resolution spatial data (2 m x 2  
21 m) to analyse the sediment connectivity in a very patchy mesoscale catchment (73 km<sup>2</sup>) of the Swiss  
22 Plateau. Specifically, we used a global sensitivity analysis to explore model structural assumptions  
23 about how linear landscape features (dis)connect the sediment cascade, which allowed us to  
24 investigate the uncertainty in the model structure. Furthermore, we compared model simulations of  
25 hillslope sediment yields from five sub-catchments to tributary sediment loads, which were calculated  
26 with long-term water discharge and suspended sediment measurements. The sensitivity analysis  
27 revealed that the assumptions about how the road network (dis)connects the sediment transfer from  
28 field blocks to water courses had a much higher impact on modelled sediment yields than the  
29 uncertainty in model parameters. Model simulations showed a higher agreement with tributary  
30 sediment loads when the road network was assumed to directly connect sediments from hillslopes to  
31 water courses. Our results ultimately illustrate how a high-density road network combined with an  
32 effective drainage system increases sediment connectivity from hillslopes to surface waters in  
33 agricultural landscapes. This further highlights the importance of considering linear landscape features  
34 and model structural uncertainty in soil erosion and sediment connectivity research.

35

## 36 **1 Introduction**

37 Rainfall events on sloped surfaces continuously displace soil particles, which are transported  
38 downslope as sediments. These sediments are then stored and remobilised several times before  
39 conceivably reaching surface waters. Accordingly, the sediment cascade is a natural and potentially  
40 long geomorphological process (Fryirs, 2013). However, the accelerated sediment supply from  
41 agricultural soils to riverine and lacustrine environments leads to negative off-site consequences.  
42 Specifically, nutrient-rich and pollutant-bound particulate matter from arable land is associated to the  
43 eutrophication and contamination of water courses (Krasa et al., 2019; Lacey et al., 2021). Extreme  
44 erosion events in agricultural fields are also linked to the occurrence of muddy floods (Boardman,  
45 2020) and to damages to downstream infrastructure (Bauer et al., 2019). Therefore, understanding how  
46 and when sediment is transferred from agricultural fields to different landscape compartments is  
47 imperative to reduce off-site erosion impacts.

48 The degree with which a system facilitates sediment transfer within its internal compartments is  
49 defined by Heckmann et al. (2018) as sediment connectivity. This concept can be further distinguished  
50 into a structural component, associated to the semi-static spatial configuration of the landscape; and a  
51 functional one, which emerges as a dynamic property of the hydro-sedimentological system  
52 (Wainwright et al., 2011). Connectivity theory therefore provides a framework to rethink the sediment  
53 delivery problem (Fryirs, 2013; Parsons et al., 2009) and to understand the complex spatio-temporal  
54 processes that regulate sediment transport.

55 In agricultural landscapes, sediment connectivity is strongly affected by the patchiness of the land use  
56 configuration, and the presence of linear features between field parcels (e.g. hedges, grass buffer  
57 strips, and roads) (Alder et al., 2015; Bakker et al., 2008; Chartin et al., 2013; Fiener et al., 2011;  
58 Remund et al., 2021; Van Oost et al., 2000). The importance of landscape patchiness in regulating  
59 sediment transfer is specifically relevant in areas where a large number of small fields, separated by  
60 linear structures, create a complex hydrological system. However, the experimental analysis of  
61 sediment connectivity at catchment scale is challenging, as it involves measuring both internal soil  
62 redistribution processes and cascading sediment transport rates. The interaction between landscape  
63 patchiness, linear structures, and sediment connectivity is therefore not addressed by the typical setup  
64 of experimental erosion studies, which either focus on small erosion plots or catchment sediment  
65 yields (Fiener et al., 2019).

66 Due to the difficulties in measuring the processes that affect sediment movement at catchment and  
67 landscape scale, it is common practice to analyse connectivity with modelling approaches (Nunes et  
68 al., 2018). These usually rely on high-resolution process-based models, assuming they are able to  
69 represent connectivity dynamics (Baartman et al., 2020); semi-qualitative indices (Borselli et al., 2008;  
70 Cavalli et al., 2013); or more recently, the coupling of conceptual models with probability theory  
71 (Mahoney et al., 2020a, 2020b). In specific, the use of process-based soil erosion and sediment

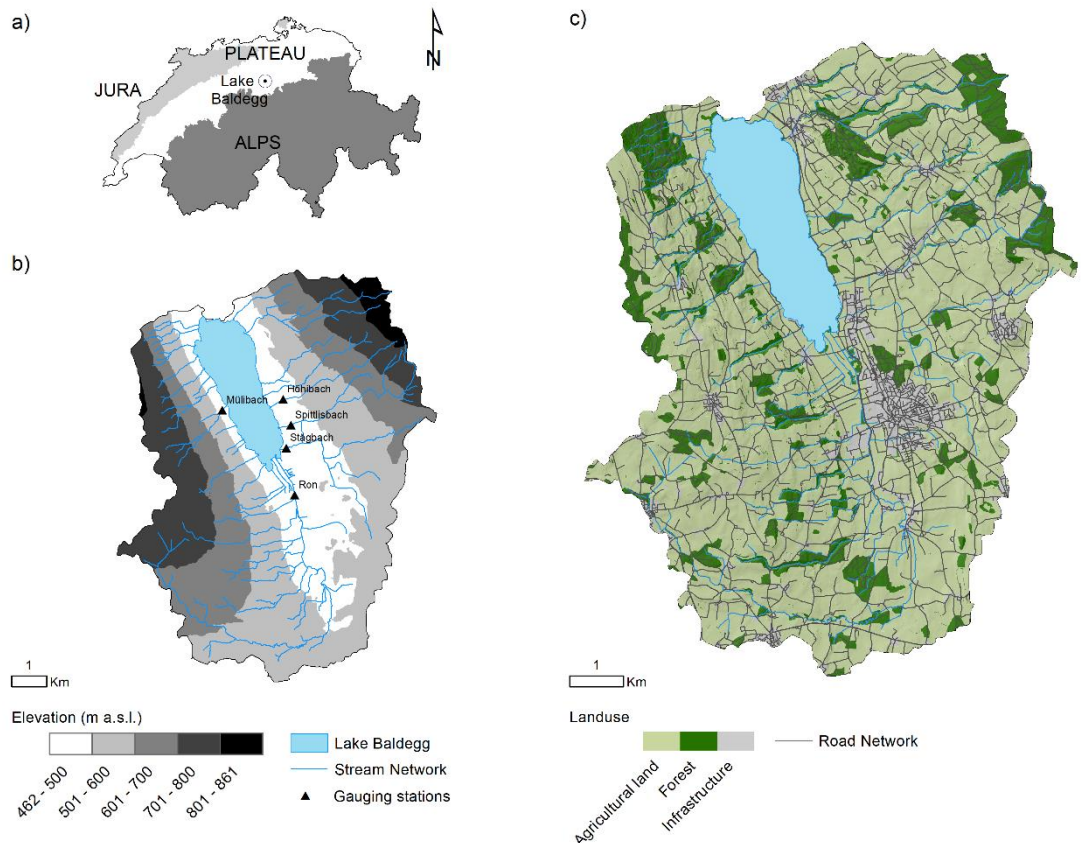
72 transport models might be an important pathway to improve our understanding of sediment  
73 connectivity (Nunes et al., 2018). However, erosion models in general, and process-based models in  
74 particular, face two fundamental problems for representing sediment connectivity : (i) the input data  
75 requirements are large and uncertain, and model application is often restricted to small catchments  
76 with a maximum size of a few square kilometres (e.g. Baartman et al., 2020; Starkloff and Stolte,  
77 2014; Wilken et al., 2017) and (ii) the implemented process descriptions, especially along linear  
78 landscape features and field boundaries, are weakly defined due to the aforementioned unavailability  
79 of experimental data. Borrelli et al. (2018) demonstrated how parcel-specific high resolution land  
80 cover and management data can improve soil erosion/sediment delivery models in patchy agricultural  
81 catchments.

82 Here, we aimed to (i) adapt a conceptual soil erosion and sediment delivery model with high spatial  
83 resolution data (2 m x 2 m) within a Monte Carlo framework; (ii) to analyse the sediment connectivity  
84 in a very patchy mesoscale catchment (73 km<sup>2</sup>) in Switzerland; and (iii) to perform a sensitivity  
85 analysis of model parameters and structural assumptions regarding how linear features (dis)connect  
86 the sediment cascade. Hence, we demonstrate how models can be used to understand the interaction  
87 between linear features, landscape patchiness, and sediment connectivity. This will contribute to  
88 increase our comprehension of relevant connectivity processes and our ability to develop appropriate  
89 measures for reducing off-site erosion impacts.

## 90 **2 Materials and methods**

### 91 **2.1 Study catchment**

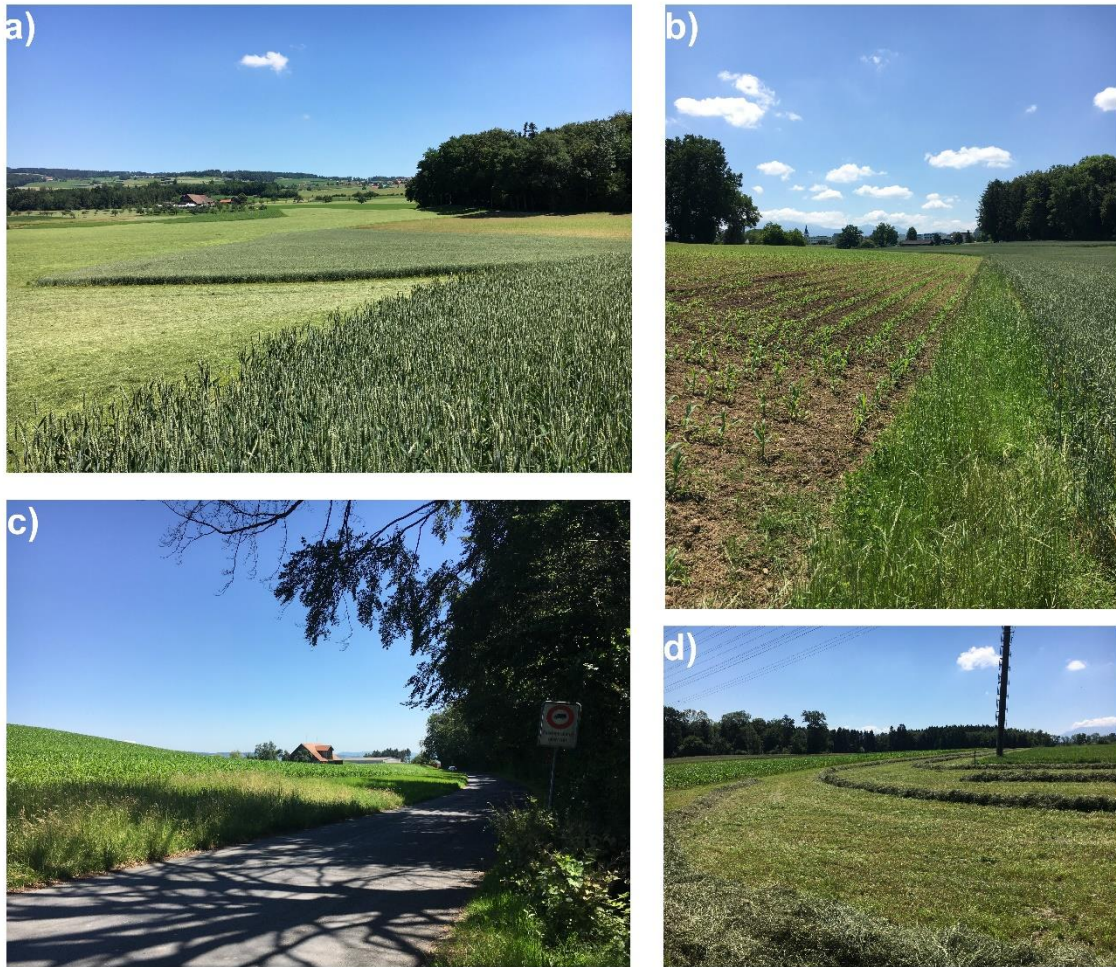
92 The study catchment consists of the contributing area of the Lake Baldegg, in the central Swiss  
93 Plateau (Figure 1). The lake has been extensively studied due to its hypertrophic waters, which have  
94 been artificially oxygenated since 1983 (e.g. Lavrieux et al., 2019; Müller et al., 2014; Teranes and  
95 Bernasconi, 2005). The eutrophication of the lake has been mostly linked to excessive phosphorus  
96 loads during the 20<sup>th</sup> century (Wehrli et al., 1997). Although water quality in the lake is currently  
97 improving (BAFU, 2016), the supply of phosphorus-rich sediment is still a concern to local authorities  
98 (von Arb et al., 2021; Stoll et al., 2019). The major advantage of the Baldegg catchment for this study  
99 is that a comprehensive hydrological data set is available based on an ongoing, long-term monitoring  
100 by the Department of Environment and Energy of the Canton of Lucerne.



101

102 Figure 1. a) Location of the Baldegg catchment; b) elevation, stream network, and location of  
 103 hydrological gauging stations; c) land use. Data source: Swisstopo, 2020. Sub-catchment areas:  
 104 Höhibach (2.3 km<sup>2</sup>), Müllbach (1.6 km<sup>2</sup>), Stägibach (9.3 km<sup>2</sup>), Spittlisbach (3.8 km<sup>2</sup>), Ron (27.7 km<sup>2</sup>).

105 The Baldegg catchment has a total area of 73.2 km<sup>2</sup>, of which 5.2 km<sup>2</sup> are covered by the lake. The  
 106 remaining area is occupied by agricultural land (74%), forests (16%), and infrastructure (e.g.  
 107 settlements, developed areas, and roads) (10%) (Swisstopo, 2020) (Figure 1c). The agriculture consists  
 108 of intensively managed pastures and/or meadows, cereal production under crop rotation, permanent  
 109 grasslands, fruit orchards, and small vineyards (Lavrieux et al., 2019; Stoll et al., 2019). The majority  
 110 of the meadows are composed of a mixture of grasses and clover, which are harvested for silage, hay,  
 111 or barn feeding up to six times per year (von Arb et al., 2021). Agricultural field blocks, here delimited  
 112 by external boundaries (e.g. roads, water courses, and forests) (Bircher et al., 2019), have a median  
 113 size of 4.4 ha. However, smaller patches separated by hedges, tree lines, and grass buffer strips, are  
 114 generally found within the blocks (Figure 2).



115

116 Figure 2. Typical agricultural landscapes from the Baldegg catchment: a) Small arable and grassland  
 117 patches within larger field blocks, b) grass buffer strip between maize and wheat fields, c) wide grass  
 118 buffer strip between maize field and a vicinal road, d) freshly cut hay from a pasture in between maize  
 119 fields.

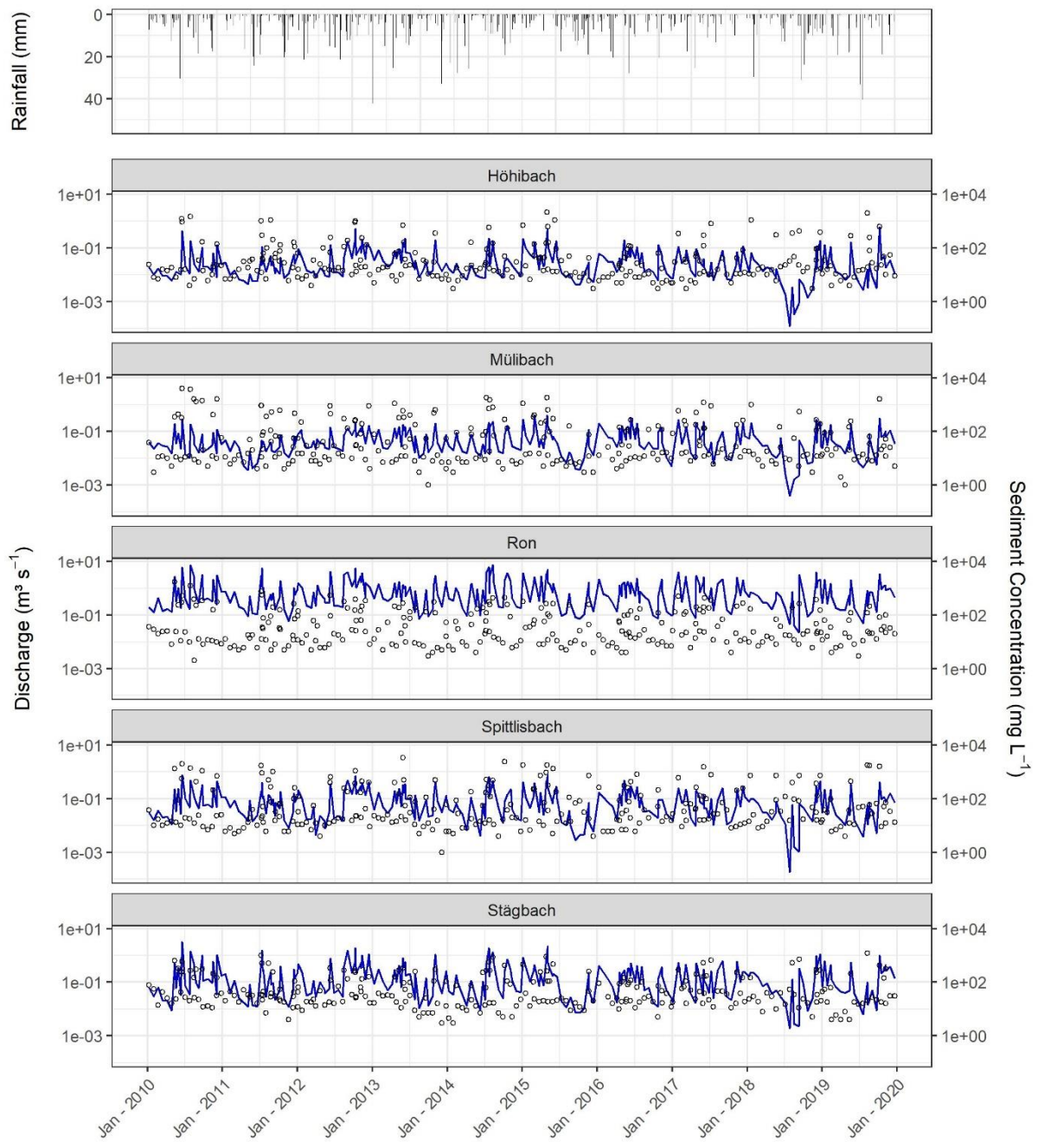
120 The road network density in the Baldegg catchment is  $6.0 \text{ km km}^{-2}$ , which is approximately three  
 121 times higher than the stream density ( $1.9 \text{ km km}^{-2}$ ). Streams in the upper catchment are often incised,  
 122 with visible, yet not prominent, signs of bank erosion. A total of 22 channels flow into the Lake  
 123 Baldegg, of which five streams are monitored for water and sediment discharge by cantonal  
 124 authorities, as described in section 2.2.

125 The elevation in the Baldegg catchment ranges from 462 to 861 m a.s.l. Steeper slopes (above 10) and  
 126 higher altitudes are found in the eastern and western sides of the catchment (Figure 1b), in a typical  
 127 glacial landscape of the Swiss Plateau – in this case formed by the retreat of the Reuss Glacier in the  
 128 south to north direction (~18,000 years BP) (Keller, 2021; Pfiffner, 2021). As a result, calcareous  
 129 Cambisols (IUSS Working Group WRB, 2006) developed upon Tertiary and Quaternary deposits are

130 the main soil class in the catchment. Rainfall is well distributed throughout the year, although greater  
131 precipitation is observed from May to August. The average annual rainfall (2010-2019) at the closest  
132 gauging station is  $\sim 1000 \text{ mm yr}^{-1}$  (Mosen, 454 m a.s.l.,  $\sim 3.5 \text{ km}$  north of the Lake Baldegg, acquired  
133 from MeteoSwiss 2021) and mean rainfall erosivity in the catchment is  $\sim 1150 \text{ MJ mm ha}^{-1} \text{ h}^{-1} \text{ yr}^{-1}$   
134 (Schmidt et al., 2016).

## 135 **2.2 Tributary suspended sediment loads**

136 Suspended sediment concentrations from five tributaries to the Lake Baldegg are monitored by the  
137 Department of Environment and Energy of the Canton of Lucerne. Here, we used the data measured  
138 from Jan 2010 to Dec 2019. On average 274 grab samples were taken from each tributary, which  
139 corresponds to one sample every 22 days, plus additional samples collected during high-flow events  
140 (10 – 13 per year) (Figure 3). Suspended sediments were measured at the same location where water  
141 discharge was monitored by automatic gauging stations (Figure 1b). A summary of the measured  
142 rainfall, water discharge, and sediment concentration from 2010 to 2019 is displayed in Figure 3.



143

144 Figure 3. Daily rainfall at the Mosen station, mean daily discharge (blue line), and sediment  
 145 concentration (circles) at the monitored tributaries of the Lake Baldegg (2010-2019). Data source:  
 146 MeteoSwiss (2021).



147 In order to calculate the sediment load for the monitored tributaries, we fitted a rating curve (Equation  
 148 1) with the measured sediment concentrations and their correspondent discharge. Additional covariates  
 149 were included to account for hysteresis, seasonality, and constituent exhaustion (Table 1) (Vigiak and  
 150 Bende-Michl, 2013; Wang et al., 2011):

$$\ln c_i = \beta_0 + \sum_{k=1}^5 \beta_k x_{k,i} + \varepsilon_i \quad (1)$$

151

152 Where:  $c$  is sediment concentration ( $\text{mg L}^{-1}$ ) for day  $i$ ,  $\beta_0$  is the intercept,  $\beta_k$  are fitted coefficients,  $x_k$   
 153 are covariates (Tab. 1) accounting for discharge, hysteresis, seasonality and constituent exhaustion,  $k$   
 154 is the covariate identification, and  $\varepsilon_i$  is the residual error.

155 Table 1. Covariates used for fitting the sediment-rating curve, as in Vigiak and Bende-Michl (2013)  
 156 and Wang et al. (2011).

Covariate	Expression	Explanation	Physical interpretation
$x_{1,k}$	$\ln Q_i$	$Q_i =$ discharge for day $i$ ( $\text{m}^3\text{s}^{-1}$ )	Discharge
$x_{2,k}$	$(\ln Q_i)^2$	Quadratic term of $x_{1,i}$	Hysteresis
$x_{3,k}$	$\sin(2\pi M_i/12)$	$M_i =$ month of day $i$	Seasonality
$x_{4,k}$	$\cos(2\pi M_i/12)$	$M_i =$ month of day $i$	Seasonality
$x_{5,k}$	$\frac{\sum_{z=1}^i 0.95^{i+1-z} Q_z}{\sum_{z=1}^i 0.95^{i+1-z}}$	Discount flow up to day $i$	Constituent exhaustion (see Wang et al., 2011)

157

158 The rating curve was used to estimate daily sediment concentrations for the entire 2010-2019 period.  
 159 Subsequently, we propagated the uncertainty in the regression fit by simulating posterior distributions  
 160 of the model coefficients ( $\beta_0, \beta_k$ ) with an informal Bayesian function of the R package ‘*arm*’ (Gelman  
 161 and Hill, 2007), as in Batista et al. (2021). The posterior distributions were used to simulate 1000  
 162 sediment concentration values for each day  $i$ . These were transformed into daily distributions of  
 163 sediment loads (Mg), considering the mean daily discharge measurements from the gauging stations.  
 164 Sediment loads were ultimately aggregated into average annual values ( $\text{Mg yr}^{-1}$ ).

### 165 2.3 Model description

166 A modified version of the spatially distributed erosion and sediment transport WaTEM/SEDEM (Van  
 167 Oost et al., 2000; Van Rompaey et al., 2001; Verstraeten et al., 2010) was used in this study.  
 168 WaTEM/SEDEM provides a framework for modelling sediment connectivity from hillslope to water  
 169 courses by use of a steady state transport capacity equation and a pixel-based sediment routing  
 170 component. That is, the model assumes that soil particles displaced by water erosion at a given grid

171 cell are transferred downstream for as long as the runoff transport capacity is greater than the sediment  
 172 supply, or until the flow path reaches a definite sink. Although the model is able to simulate both  
 173 tillage and water erosion, here we focus on the latter, which is calculated with an adaptation of the  
 174 RUSLE (Renard et al., 1997) (Equation 2). We chose to focus on soil erosion by water because in  
 175 WaTEM/SEDEM the sediment supply/routing is not affected by tillage erosion. However, tillage  
 176 erosion is likely to be an important within-field soil redistribution process in the catchment (please see  
 177 discussion below). The model is by default executed in an average yearly time step, as typical in  
 178 RUSLE applications:

179

$$A = R K LS_{2d} C P \quad (2)$$

180

181 Where:  $A$  is average annual soil loss ( $\text{kg m}^{-2} \text{yr}^{-1}$ ),  $R$  is rainfall erosivity ( $\text{MJ mm m}^{-2} \text{h}^{-1} \text{yr}^{-1}$ ),  $K$  is soil  
 182 erodibility ( $\text{kg h MJ}^{-1} \text{mm}^{-1}$ ),  $LS_{2d}$  is a topographic factor calculated by the Desmet and Govers (1996)  
 183 procedure (dimensionless),  $C$  is a cover-management factor (dimensionless), and  $P$  is a support  
 184 practice factor (dimensionless).

185 Transport capacity ( $\text{kg m}^{-1} \text{yr}^{-1}$ ) per unit widths of grid cells is assumed to be proportional to the  
 186 potential to rill erosion, which is described by a power function of slope length and gradient (Van  
 187 Rompaey et al., 2001):

188

$$TC = K_{TC} R K (LS_{2d} - 4.12 S_g^{0.8}) \quad (3)$$

189

190 Where:  $K_{TC}$  is a landuse-dependent transport capacity coefficient (m) which requires calibration,  $R$  is  
 191 rainfall erosivity ( $\text{MJ mm h}^{-1} \text{yr}^{-1}$ ),  $K$  is soil erodibility ( $\text{t h MJ}^{-1} \text{mm}^{-1}$ ),  $LS_{2d}$  is a topographic factor  
 192 calculated by the Desmet and Govers (1996) procedure (dimensionless), and  $S_g$  is slope gradient ( $\text{m m}^{-1}$ ).  
 193

194 WaTEM/SEDEM partially incorporates the influence of the landscape structure on sediment transfer  
 195 by the use of a parcel connectivity parameter  $P_{Con}$ , which represents the proportion of sediment that is  
 196 stopped at field borders. The model also simulates runoff connectivity by means of a parcel trapping  
 197 efficiency  $P_{TEf}$  parameter, which corresponds to the proportion of the flow accumulation that is routed  
 198 downstream. Finally, the model is able to estimate the total amount of sediment transferred from  
 199 hillslopes to water courses, which can be interpreted as the hillslope component of a catchment  
 200 sediment budget. Since WaTEM/SEDEM does not represent gully and bank erosion, nor in-stream  
 201 erosion and deposition processes, any comparison between modelled sediment yields and catchment-  
 202 outlet sediment loads must be interpreted with caution. However, in catchments where rill and interrill

203 are the main overland erosion processes, and assuming a state of long term fluvial quasi equilibrium,  
204 the outlet sediment loads should be at least comparable to the model outputs – even if not fully  
205 commensurable. For further information on the model, we refer to Notebaert et al., (2006), Van Oost  
206 et al., (2000), Van Rompaey et al., (2001), and Verstraeten et al., (2010).

#### 207 **2.4 Model implementation, input data, and sensitivity analysis**

208 WaTEM/SEDEM is implemented as a user friendly GUI developed at KU Leuven (Notebaert et al.,  
209 2006). Although the software facilitates model application, it does not allow for more complex  
210 operations, such as sensitivity or uncertainty analysis. Moreover, some model components might not  
211 be fully comprehensible without access to the source code, and WaTEM/SEDEM is frequently used as  
212 a black box. Hence, in order to perform a sensitivity analysis of model parameters and underlying  
213 structural model assumptions, we implemented a WaTEM/SEDEM version using the free open source  
214 software R (R Core Team, 2021) and SAGA GIS (Conrad et al., 2015). The main adaptations are  
215 described in the following, and our code is available as supplementary material.

216 Our model application consists of a global all-at-a-time sensitivity analysis, as described by Pianosi et  
217 al. (2016). That is, we performed a Monte Carlo simulation to explore the variability of the whole  
218 parameter space, and all input factors were sampled simultaneously for each model realisation ( $n =$   
219 1200). The framework is similar to an uncertainty analysis, except in this case we did not focus on  
220 locating the parameter space which produced behavioural model realisations. Instead, we concentrated  
221 on apportioning sources of uncertainty to different model input factors, aiming to rank their  
222 contribution to the variability of the response surface (see Pianosi et al., 2016 for a review on  
223 sensitivity analysis). This should allow us to identify parameters and model assumptions that have a  
224 greater impact on the manner with which WaTEM/SEDEM describes sediment connectivity in the  
225 Baldegg catchment. In particular, the analysis of different assumptions about the structure of the  
226 model should provide a connectivity assessment based on the quantification of the structural  
227 uncertainty within the simulations. To the best of our knowledge, this is the first time the analysis of  
228 model structural error is incorporated to sediment connectivity research.

229 For each iteration of the Monte Carlo simulation, all RUSLE input variables were sampled from  
230 uniform distributions, except for the  $LS_{2d}$  factor (Table 2). Minimum and maximum  $R$  factor values  
231 were retrieved from the Swiss national map (Schmidt et al., 2016), and a single lumped value for the  
232 whole catchment was sampled for each iteration. The same approach was used for the  $K$  factor  
233 (Schmidt et al., 2018a). We used lumped catchment values for these factors due to their low spatial  
234 variability within the study area, according to the national maps (coefficient of variations are 1% and  
235 7% for the  $K$  and  $R$  factor, respectively). For the  $C$  and  $P$  factors, here combined in a single  $CP$   
236 parameter, uniform distributions were created for each landuse class in the catchment, based on  
237 commonly used values from the literature and a land cover map (1:25000) (Swisstopo, 2020), which  
238 we rasterised to the model resolution (2 m x 2 m). Due to the unavailability of open source geodata of

239 crop statistics in the Baldegg catchment, pastures and cropland were aggregated into a single arable  
240 land category (Table 2). In this case, minimum and maximum values were relaxed to represent a wide  
241 possible combination of crops and support practices. Such combinations were assessed with the *CP*-  
242 Tool (Kupferschmied, 2019), which allows for the calculation of *CP* values considering common crop  
243 rotation systems in Switzerland. The minimum *CP* values were particularly reduced to include typical  
244 values for permanent grasslands in Switzerland (~0.01) (Schmidt et al., 2018b). Finally, the *LS<sub>2d</sub>* factor  
245 was calculated with a slope (rad) and an upslope contributing area (m<sup>2</sup>) grid, which were obtained by  
246 processing a 2 m x 2 m resolution DEM from SwissALTI3D (Swisstopo, 2014a).

247 Table 2. Minimum and maximum parameter values sampled during the Monte Carlo simulation.

Parameter	Category	Min	Max
$R$ (MJ mm m <sup>-2</sup> h <sup>-1</sup> yr <sup>-1</sup> )		950 10 <sup>-4</sup>	1350 10 <sup>-4</sup>
$K$ (kg h MJ <sup>-1</sup> mm <sup>-1</sup> )		0.025 10 <sup>3</sup>	0.040 10 <sup>3</sup>
$CP$ (-)	Arable land	0.01	0.5
	Grass buffer strips	0.001	0.009
	Forest	0.0001	0.003
	Orchard	0.001	0.2
	Vineyard	0.05	0.6
$K_{TC}$ (m)	High (arable land, vineyard)	1	200
	Low (grass buffer strips, forest, orchard)	1	100
$P_{TEf}$ (-)		0	1
$P_{Con}$ (-)		0	1

248

249 Similarly, all WaTEM/SEDEM-specific model parameters were sampled from uniform distributions  
 250 (Table 2). Landuse classes with a  $CP$  factor above 0.01 received higher transport capacity coefficients  
 251 ( $K_{TC}$  high). The remaining landuse classes, namely forests and grass strips, received lower coefficients  
 252 ( $K_{TC}$  low). The  $K_{TC}$  reference values were taken from Van Rompaey et al. (2001) and extended in order  
 253 to explore a larger parameter space. The sampled parcel trapping efficiency ( $P_{TEf}$ ) values were  
 254 assigned to forests and grass buffer strips in the rasterised land cover map, as we explain below. The  
 255 resulting  $P_{TEf}$  grid was used as a weight for calculating the aforementioned upslope contributing area.  
 256 Hence, only a proportion of the grid-cell area from forests and grass strips contributed to the  
 257 downstream flow accumulation, as runoff amounts are assumed not to increase (or to increase slowly)  
 258 with slope length under natural vegetation (Govers, 2011). Parcel connectivity ( $P_{Con}$ ) values were  
 259 assigned to the forest and grass buffer strips cells that bordered agricultural fields, representing the  
 260 extent with which water and sediment transport is reduced at parcel borders (Notebaert et al., 2006).  
 261 The transport capacity (Eq. 2) at these cells was reduced by a fraction inversely proportional to the  
 262 sampled  $P_{Con}$  value.

263 For each sampled combination of parameters values, the models were ran with and without the  
 264 presence of grass buffer strips between agricultural field blocks and adjacent roads and forests.  
 265 Although grass buffer strips are generally present at field borders in the Baldegg catchment (Figure 2),  
 266 these features were not distinguishable in the land cover map. Hence, we manually inserted 2 m wide  
 267 grass buffer strips at the aforementioned borders. The extent of the buffer-strips in reality is quite  
 268 variable, and generally wider at forest and river vicinities (3 – 6 m), as required by law in Switzerland  
 269 (Alder et al., 2015). For simplicity, we used a single value that should allow us to test the sensitivity of  
 270 the model to the presence of the strips. The 2 m width was selected based on the spatial resolution of  
 271 the model input data. On the other hand, hedges and tree lines within field blocks were already  
 272 classified in the land cover map and required no additional processing.

273 Furthermore, three road connectivity assumptions were assessed for each model iteration. In a first  
274 scenario, roads were treated as an ultimate sink, with zero transport capacity (i.e. ‘roads as sinks’).  
275 Hence, sediments reaching roads or infrastructure were subsequently removed from the system and did  
276 not reach surface waters. This represents a scenario in which roadside ditches and the road drainage  
277 system trap most sediments and partly diverge runoff to wastewater treatment plants. A second  
278 scenario assumed that all sediments reaching the road network were directly connected to the stream  
279 network. This represents a situation in which the road drainage system acts as a hydraulic shortcut,  
280 transferring sediments from fields into surface waters (i.e. ‘roads as shortcuts’) (see Schönenberger  
281 and Stamm, 2021). As in the original model formulations (see Notebaert et al., 2006), the third  
282 scenario assigned very high transport capacity to roads and infrastructure, so that no deposition would  
283 take place (i.e. ‘roads as patch connectors’). In this case, runoff and sediment might flow along or  
284 across the road network – which is expected to happen during extreme rainfall events when the  
285 drainage system is clogged. For this scenario, deposition will never occur on road cells, however  
286 sediments can still be deposited on lower patches before reaching the stream network. Hence,  
287 sediment transfer will be entirely dependent on the flow direction calculated from the DEM. Here we  
288 employed a multiple flow direction algorithm, which was used for calculating upslope contributing  
289 area and routing sediments along the flow path. The sediment routing component was implemented  
290 with a capacity accumulation function from SAGA GIS (Conrad et al., 2015), and all geo-processing  
291 tools were applied with the ‘RSAGA’ package (Brenning et al., 2018).

292 The sensitivity of WaTEM/SEDEM to the uncertainty in model parameters, the presence of grass  
293 buffer strips, and assumptions about road connectivity (i.e., model structural uncertainty) was assessed  
294 by evaluating modelled hillslope sediment yields (i.e., the amount of sediment delivered from  
295 hillslopes to surface waters) for the entire Baldegg catchment. A qualitative analysis was performed  
296 with a visual inspection of scatter plots, comparing the univariate parameter space with the model  
297 response surface. Additionally, we used a random forest analysis (RFA) to rank the importance of  
298 input factors to the uncertainty in model outputs (Antoniadis et al., 2021). That is, a random forest was  
299 used to predict the WaTEM/SEDEM-modelled sediment yields, based on the sampled parameter  
300 values for each iteration of the Monte Carlo simulation. The importance of the input factors, including  
301 model parameters, the presence of grass-strips, and the road connectivity scenarios, was ranked based  
302 on their relative contribution to the RFA predictive error, following an out-of-bag estimate (Breiman,  
303 2001). We chose the RFA due to its ability to rank both qualitative and quantitative input factors. The  
304 analysis was performed with the ‘randomForest’ (Liaw and Wiener, 2002) R package.

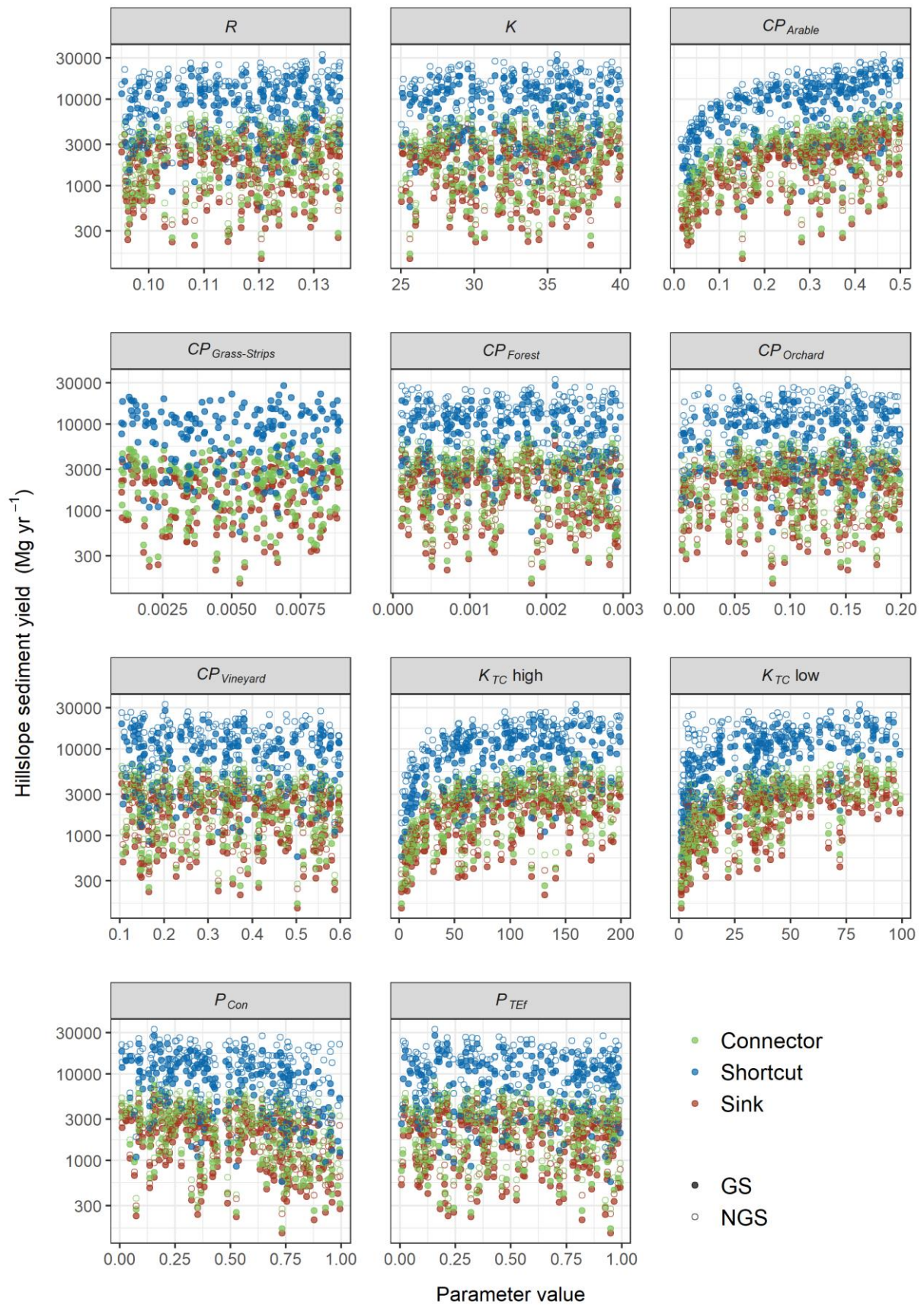
305 Finally, we compared the resulting WaTEM/SEDEM simulations of sub-catchment hillslope sediment  
306 yields to the suspended sediment loads from the monitored tributaries. Of note, with this comparison  
307 we only aim to provide a general picture of the plausibility of the model realisations. Suspended  
308 sediment loads are a product of a complex interaction of hillslope and channel remobilisation

309 processes, which are not fully represented by WaTEM/SEDEM. Hence, modelled hillslope yields and  
310 suspended loads are not entirely commensurable, and we did not focus on a rejectionist framework for  
311 model testing. This research is exploratory and investigates the importance of linear features and  
312 landscape patchiness on sediment connectivity.

### 313 **3 Results**

#### 314 **3.1 Sensitivity analysis**

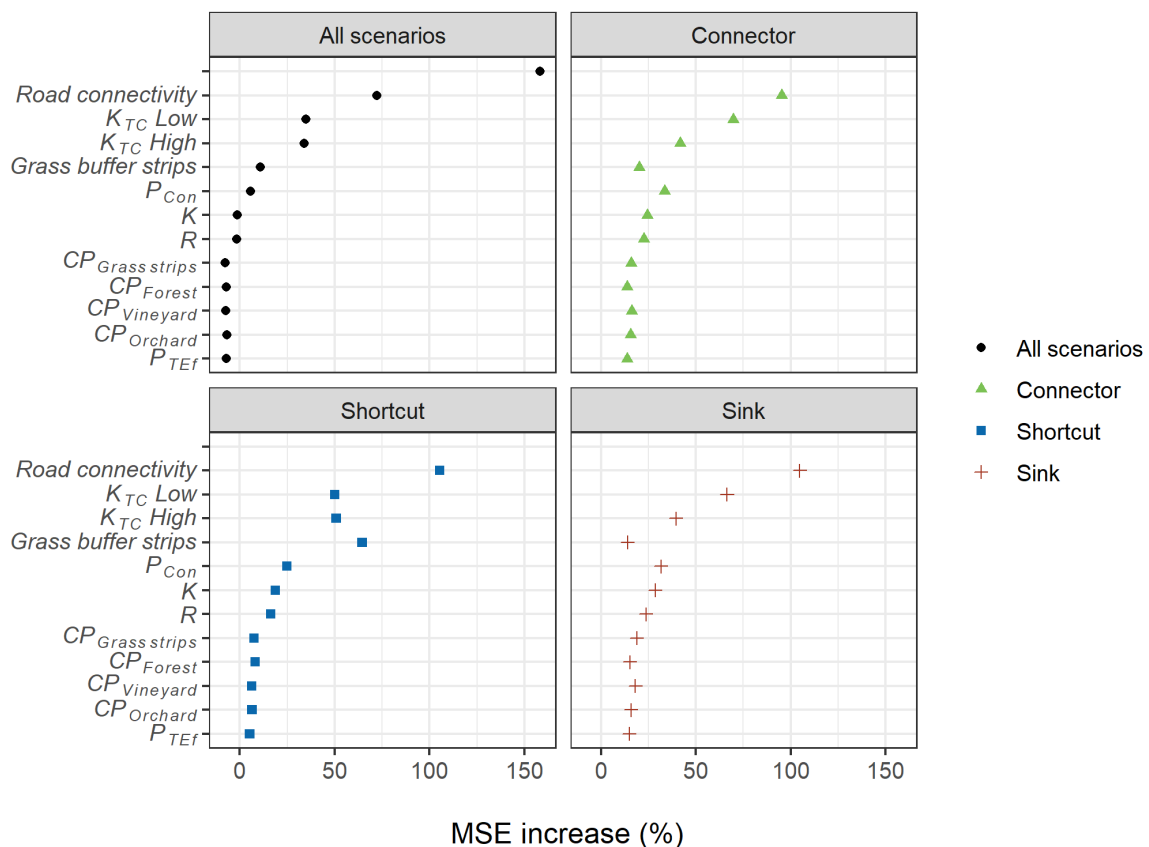
315 The road connectivity assumptions were by far the most sensitive input factor for WaTEM/SEDEM in  
316 the Baldegg catchment. This is illustrated in Figure 4, which presents scatter plots comparing sampled  
317 parameter values and the model response surface. The uniformly scattered points denote a low  
318 sensitivity of the modelled hillslope sediment yields to most input factors, with some evident  
319 exceptions:  $CP$  for arable land,  $K_{TC}$  high, and  $K_{TC}$  low. On the other hand, all plots demonstrate that  
320 higher sediment yields were calculated when we assumed that roads behaved as hydraulic shortcuts,  
321 directly connecting agricultural patches to the stream network.





325 strips (NGS). Colours represent the road connectivity assumptions (i.e. 'roads as patch connectors',  
326 'roads as hydraulic shortcuts', and 'roads as sinks'). See section 2.4 for a description of road  
327 connectivity scenarios.

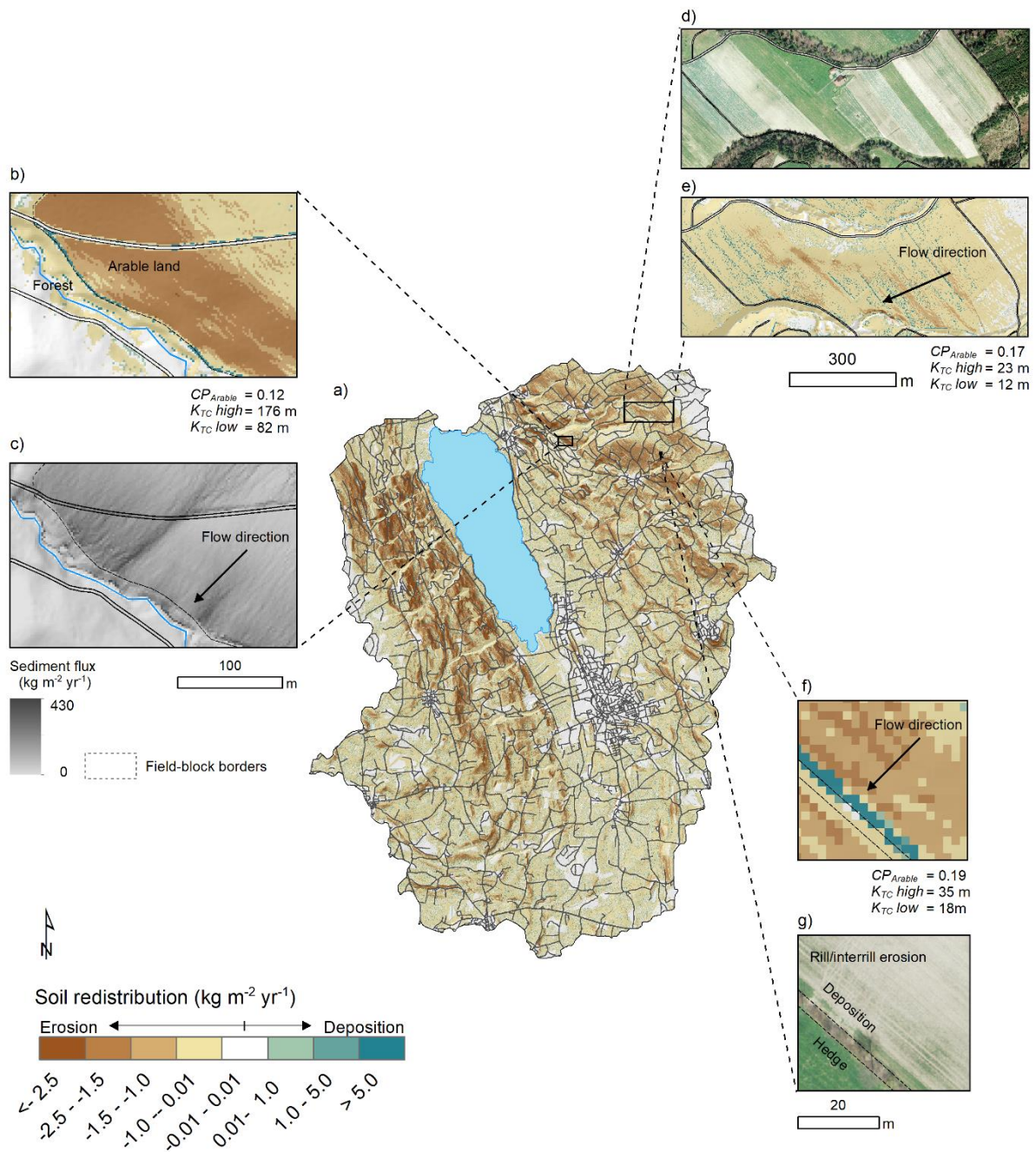
328 Similarly, the results from the RFA demonstrate that road connectivity was the most important input  
 329 factor for predicting the WaTEM/SEDEM outputs (Figure 5). That is, if road connectivity was not  
 330 considered, the predictive mean squared error (MSE) of the RFA increased by 158%. The MSE  
 331 increase associated to  $CP$  for arable land (72%),  $K_{TC}$  low (35%),  $K_{TC}$  high (34%), and the presence of  
 332 grass buffer strips (11.0%), indicate the model was also sensitive these input factors. However, if we  
 333 considered each road connectivity scenario individually, the results from the random forest were  
 334 shifted, as the model seemed to be more sensitive to the presence of grass buffer strips for the ‘road as  
 335 shortcuts’ scenario (MSE increase = 65%).



336  
 337 Figure 5. Mean squared error (MSE) increase associated to model input factors for the RFA. Larger  
 338 relative errors indicate the input factors were more important for estimating model outputs.

### 339 3.2 Spatial patterns

340 The spatial patterns of soil redistribution rates were also highly influenced by linear features,  
 341 landscape patchiness, and connectivity assumptions. Sediment deposition on field blocks downslope  
 342 from roads was more frequently observed for the ‘roads as connectors’ scenario, than for the other  
 343 road connectivity assumptions. Specifically, when sediments were not diverged or trapped by the road  
 344 network, there was a greater proportion of sediment deposition on footslope field borders and other  
 345 potential sinks (Figure 6b).



347

348 Figure 6. a) Catchment patterns of soil redistribution for a model realisation with the presence of grass  
 349 buffer strips; b) detail of sediment deposition on field borders, ‘road as patch connectors’ scenario; c)  
 350 detail of sediment fluxes across the road network, ‘road as patch connectors’ scenario’; d) detail of  
 351 aerial image of multiple parcels within a field block (Swisstopo, 2014b); e) soil redistribution rates for  
 352 the field block; f) detail of sediment deposition at a grass buffer strip at a field border; g) aerial image  
 353 for the field (Swisstopo, 2014b).

354

355 The sediment flux from agricultural fields was generally interrupted when entering forest patches, and  
 356 further deposition was modelled at forested valley floors, near the stream channels, for all scenarios  
 357 (Figure 6b, c). Importantly, sediment deposition along grass buffer strips, hedges, and tree lines  
 358 reduced sediment fluxes in between field blocks, forming a patchy connectivity pattern. This was  
 359 again visible for all simulated connectivity assumptions, albeit particularly pronounced when the  
 360 presence of grass buffer strips was considered (Figure 6 a, f).

361 Unexpectedly, the soil redistribution patterns revealed that WaTEM/SEDEM simulated linear  
 362 deposition areas at the borders of small cropland patches (Figure 6d, e). This occurred even in the  
 363 absence of grass buffer strips or hedges, and hence without  $P_{Con}$  parameterisation, which was only  
 364 applied to field-block borders. These depositional patterns were particularly evident within field  
 365 blocks oriented across the slope direction, and apparently stem from small scale changes in the slope  
 366 gradient, which were represented by the high-resolution DEM and which potentially results from long  
 367 term tillage erosion.

### 368 3.3 Soil redistribution rates, hillslope sediment-yields, and suspended sediment loads

369 Soil redistribution rates for eroding grid cells in the Baldegg catchment were almost identical among  
 370 the simulated road connectivity assumptions (Table 3). Higher absolute deposition rates were  
 371 calculated for the simulations without grass strips for both the connector and sink scenarios, which is a  
 372 result of increased erosion rates calculated without the presence of the strips. On the other hand, lower  
 373 sediment yields were calculated with the presence of grass buffer strips when the connectivity  
 374 scenarios were analysed individually. Among these scenarios, deposition rates were lower if roads  
 375 were considered to behave as hydraulic shortcuts. Contrarily, deposition rates for the ‘roads as  
 376 connectors’ and ‘roads as sinks’ scenarios were very similar, although road deposition was only  
 377 modelled in the second case. Therefore, deposition rates within fields, patch borders, colluviums, and  
 378 valley floors for the connector scenario were ~30% higher than for the other simulations. As the  
 379 sediments not diverged by the road network were ultimately deposited within the catchment, the sink  
 380 and connector scenarios displayed very similar hillslope sediment yields. Contrarily, sediment yields  
 381 for the shortcut scenario were in general ~4.5 times higher than for the remaining road connectivity  
 382 simulations.

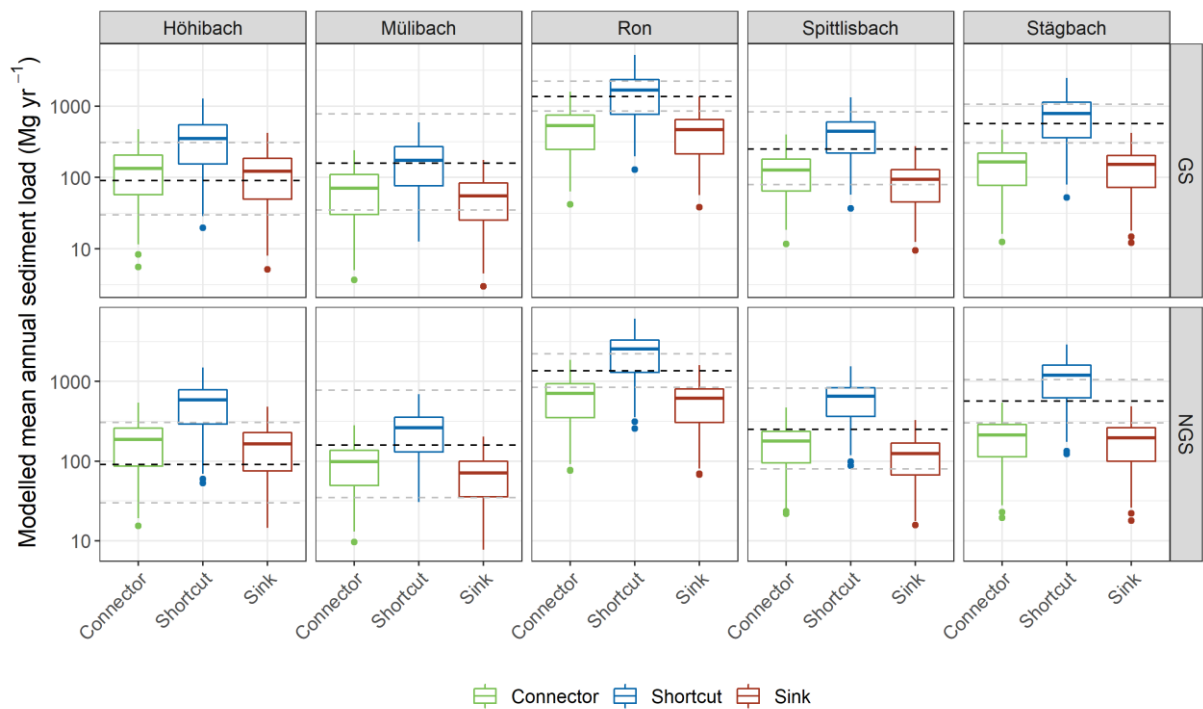
383 Table 3. Summary statistics of soil redistribution rates, hillslope sediment yields calculated by the  
 384 WaTEM/SEDEM simulations.

Scenario	Erosion			Deposition			SSY			SY			
	----- Mg ha <sup>-1</sup> yr <sup>-1</sup> -----									----- Mg yr <sup>-1</sup> -----			
	Q1	Q2	Q3	Q1	Q2	Q3	Q1	Q2	Q3	Q1	Q2	Q3	
Connector	GS	3.5	6.3	8.7	3.4	5.9	8.3	0.2	0.3	0.5	1,047	2,248	3,307
	NGS	3.7	6.6	9.1	3.5	6.1	8.5	0.2	0.4	0.6	1,498	3,054	4,097
Shortcut	GS	3.5	6.3	8.8	2.7	4.9	7.2	0.6	1.2	1.8	3,878	8,467	12,242

	NGS	3.7	6.6	9.2	2.5	4.7	6.7	0.9	1.9	2.6	6,303	13,238	17,506
	GS	3.5	6.3	8.8	3.4	6.0	8.4	0.1	0.3	0.4	833	1,828	2,665
Sink	NGS	3.7	6.6	9.2	3.5	6.2	8.7	0.2	0.4	0.5	1,143	2,389	3,197

385 SSY: area specific hillslope sediment yield; SY: hillslope sediment yield. Deposition rates include  
 386 hillslope and road deposition. GS: grass buffer strips; NGS: no grass buffer strips; Q1: first quartile, or  
 387 the 25<sup>th</sup> percentile; Q2: second quartile, or the median; Q3: third quartile, or the 75<sup>th</sup> percentile.

388 The comparison between WaTEM/SEDEM simulations and the tributary sediment loads revealed a  
 389 larger overlap between the latter and the results from the ‘road as shortcuts’ scenario (Figure 7). The  
 390 overlap became particularly clear when we compared the prediction intervals of the calculations  
 391 (Figure 7). That is, a smaller proportion of the ‘road as connectors’ and the ‘road as sinks’ model  
 392 realisations encompassed the tributary sediment loads, except for the Höhibach, which showed the  
 393 opposite pattern. This behaviour was particularly evident for the scenario with the presence of grass  
 394 buffer strips.



395  
 396 Figure 7. Box-plots of hillslope sediment loads simulated by WaTEM/SEDEM for the road  
 397 connectivity scenarios for each tributary sub-catchment. Dashed lines represent the median (in black)  
 398 and the 95% interval (in grey) of the measurement-based estimates of sediment loads for each  
 399 tributary, calculated from the error propagation of the sediment-rating curve. GS: grass buffer strips,  
 400 NGS: no grass buffer strips. Simulations for the shortcut scenario generally shows a higher overlap  
 401 with calculated sediment loads, in particular when grass buffer strips are considered.

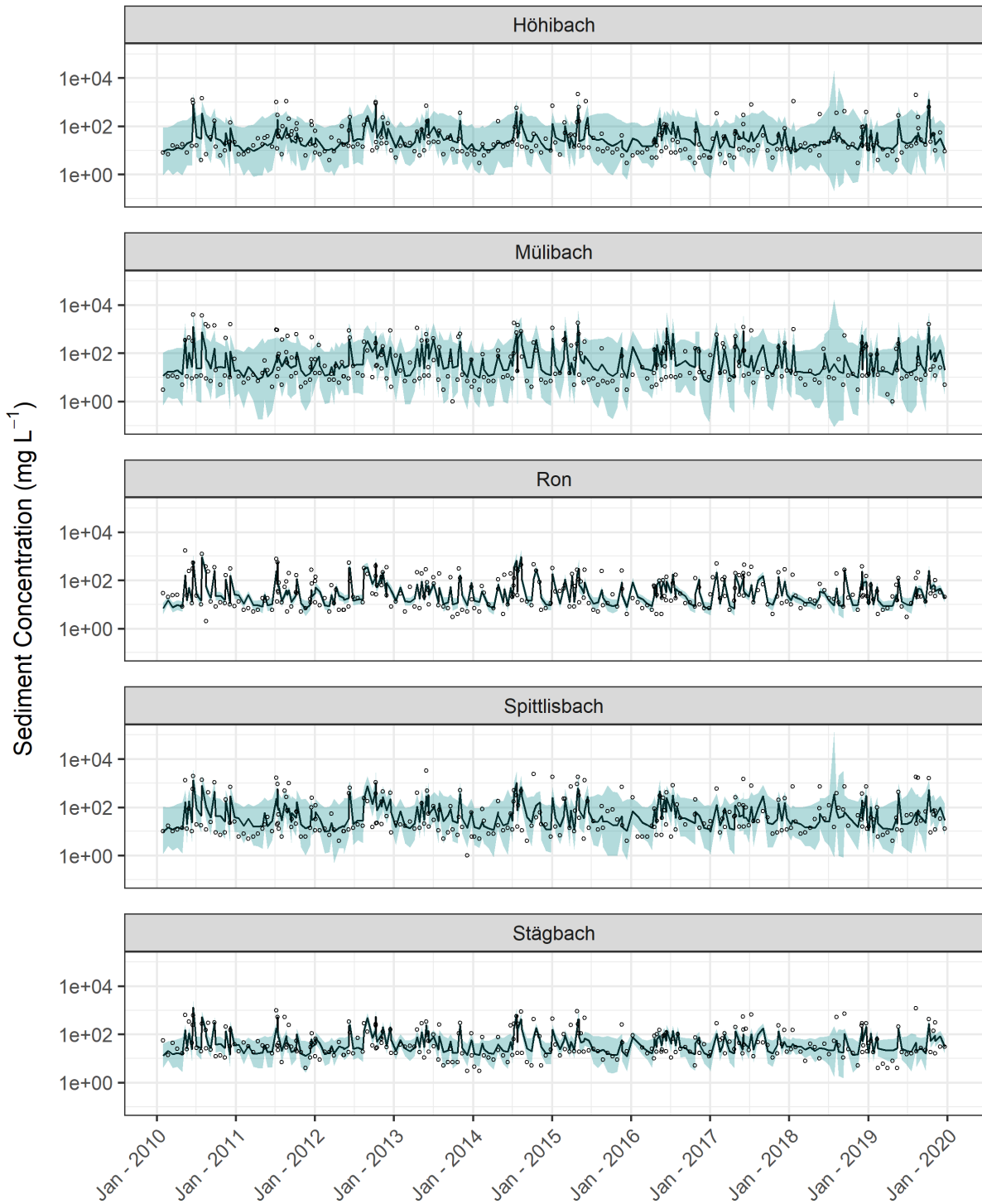
402 It is important to note that the median sediment concentrations calculated by the rating curve  
 403 (Equation 1) underestimated the actual observations, for all tributaries. This is expressed by the  
 404 positive mean error of the estimates (Table 4). Moreover, the Nash-Sutcliffe model efficiency

405 coefficient for the median calculations was unsatisfactory considering the usual thresholds for model  
 406 performance (e.g. Moriasi et al., 2015). On the other hand, the 95 % prediction interval of the rating  
 407 curve encompassed a large proportion of the observations, and most errors were associated to extreme  
 408 events (Table 4, Figure 8). Hence, it is likely that actual sediment loads from the tributaries are  
 409 contained within the long right side of the skewed distributions resulting from the error propagation of  
 410 the rating curves (Figure 7), which would increase the overlap with the shortcut scenario.

411 Table 4. Evaluation metrics of the sediment rating curve, considering the measured sediment  
 412 concentrations and median of the simulations.

Stream	ME ----- mg L <sup>-1</sup> -----	RSME	Out of bound percentage* ----- % -----	r <sub>p</sub> -----	r <sub>s</sub> -----	NSE
Höhibach	50.10	80.60	13	0.52	0.64	0.22
Mülibach	72.97	138.32	11	0.64	0.73	0.34
Ron	22.00	54.61	61	0.63	0.77	0.38
Spittlisbach	95.67	149.78	22	0.51	0.67	0.20
Stägbach	25.05	67.14	36	0.50	0.70	0.19

413 \*percentage of observations out of the 95 % prediction interval. ME: mean error; RMSE: root-mean-  
 414 square error, r<sub>p</sub>: Pearson's correlation coefficient, r<sub>s</sub>: Spearman's correlation coefficient; NSE: Nash-  
 415 Sutcliffe model efficiency coefficient.



416

417 Figure 8. Log-scaled daily sediment concentrations estimates from the rating curve: dark solid line is  
 418 the median of the calculations and the shaded light blue represents the 95 % prediction interval. Open  
 419 circles are the observed values used for fitting the curve.

420 **4 Discussion**

421 Here we assessed the interaction between landscape patchiness, linear structures, and sediment  
 422 connectivity. Our quantitative model-based approach highlighted the importance of roads in

423 (dis)connecting sediment fluxes between landscape compartments and surface waters in patchy  
424 agricultural catchments. These findings are in lines with long-term field observations and qualitative  
425 model assessments for similar areas in Switzerland.

426 For instance, Ledermann et al. (2010) monitored off-site erosion in multiple fields from different  
427 regions of the Swiss midlands and found that linear features in general and roads in particular had a  
428 large influence on runoff concentration, soil erosion rates, and off-site damage. These authors also  
429 estimated that > 50 % of eroded soil was deposited in adjacent fields and infra-structure, while up to  
430 20 % reached surface waters, mainly through indirect inflow via the road and drainage network. Such  
431 figures are proportionate to WaTEM/SEDEM estimations for the Baldegg catchment, specifically for  
432 the shortcut scenario with the presence of grass buffer strips (Table 3). Another interesting similarity  
433 between our outputs and the field assessments from Ledermann et al. (2010), was that both approaches  
434 identified field border structures as critical regulators of soil erosion and sediment transport (see  
435 Figures 5 and 6). According to the field assessments, border furrows are specifically important for  
436 both triggering erosion and promoting diffuse sediment deposition. Such features, combined with  
437 long-term tillage erosion, might be responsible creating the topographic pattern displayed in Figure 6d.

438 Moreover, the capacity of roads to connect runoff and sediments from arable land to surface waters in  
439 Switzerland was extensively described by Alder et al. (2015) and Schönenberger and Stamm (2021).  
440 Both studies used a similar semi-qualitative modelling approach for identifying agricultural fields that  
441 were directly or indirectly (i.e. via the road and drainage networks) connected to surface waters. In  
442 particular, Schönenberger and Stamm (2021) mapped the location of drainage inlets in multiple small  
443 catchments of the Swiss Plateau. Accordingly, these authors identified the road drainage system as the  
444 main hydraulic shortcut connecting fields to water courses, as most drainage inlets discharge into  
445 surface waters (87%), and only a small proportion of them flow into wastewater treatment plants or  
446 depositional areas. Hence, the fact that the WaTEM/SEDEM ‘road as shortcuts’ scenario displayed a  
447 greater agreement with the sediment rating curves for the Baldegg tributaries (Figure 7) is coherent  
448 with the current understanding of runoff dynamics in the Swiss Plateau. Of note, the contrasting  
449 results for the Höhibach sediment loads (Figure 7), which are much closer to the sink and patch-  
450 connector simulations, do not seem to be explained by any physiographical characteristic of the sub-  
451 catchment (e.g. stream and road density, slope, or land cover). Hence, we speculate that this different  
452 pattern could be caused by a lower inlet drainage density or cropping specificities in the Höhibach  
453 contributing area.

454 In addition, our simulations of edge-of-field grass buffer strips indicated that these structures might be  
455 particularly relevant for the ‘road as shortcuts’ scenario. In this case, the model estimated that grass  
456 trips could reduce up to 30% the sediment connectivity from hillslopes to surface waters in the  
457 Baldegg catchment (Table 4). However, it should be noted that we assumed 2 m wide strips at field  
458 block borders, irrespectively of the adjacent structures or land use. As previously mentioned, the



459 extent of these features is in fact quite variable, and legislation only requires 0.5 m filters between  
460 fields and roads, as reported by Alder et al. (2015). These authors further emphasised that albeit edge-  
461 of-field strips are an important complementary management practice, their effectiveness is often  
462 reduced in case of large drainage areas, in which very wide buffers would be necessary to stop  
463 sediment fluxes. Hence, Alder et al. (2015) recommended that minimising on-site erosion rates was  
464 ultimately the most effective way to decrease sediment input from arable land to water courses in  
465 Switzerland. Our results support this management proposition. However, our simulations also indicate  
466 that the disproportional sediment connectivity afforded by the dense road network translates into an  
467 excessive sediment supply to water courses, even when simulated erosion rates were small. As on-site  
468 erosion rates in Switzerland are already reasonably low (see Prasuhn, 2020), it might be important to  
469 consider solutions that address the sediment transport through the underground drainage system,  
470 particularly in environmentally sensitive areas, such as the Baldegg catchment.

471 In a wider context, our study has demonstrated how structural sediment connectivity patterns can be  
472 investigated with a conceptual model as WaTEM/SEDEM, provided that model resolution is  
473 sufficiently fine to represent relevant features and processes. In agricultural catchments of the Swiss  
474 Plateau and likely in other patchy landscapes, soil redistribution rates and patterns are intrinsically  
475 linked to linear features (see Alder et al., 2015; Ledermann et al., 2010; Prasuhn, 2020; Remund et al.,  
476 2021). Hence, in order to provide relevant system descriptions, soil erosion models applied under  
477 similar conditions must be able to represent linear features and landscape patchiness. Although our  
478 results might seem case-specific, similar findings have been reported around the world. For instance,  
479 the effects of roads and farm tracks in both coupling and decoupling runoff and sediments has been  
480 described in Australia (Croke et al., 2005), Brazil (Bispo et al., 2020), Kenya (Stenfert Kroese et al.,  
481 2020), Italy (Persichillo et al., 2018), Spain (Calsamiglia et al., 2018), and the USA (Mahoney et al.,  
482 2018). Moreover, the influence of linear features such as field borders, hedges, terraces, and tractor  
483 tram lines on soil redistribution rates have been well documented in Europe (Calsamiglia et al., 2018b;  
484 Evrard et al., 2009; Fiener and Auerswald, 2005; Lacoste et al., 2014; Saggau et al., 2019), as well as  
485 the importance of landscape structure in regulating sediment connectivity (Baartman et al., 2020;  
486 Chartin et al., 2013; Fiener et al., 2011).

487 Another generalisable finding from our research was that WaTEM/SEDEM can be as sensitive to  
488 RUSLE parameters as to the model-specific transport capacity coefficients. Therefore, when  
489 performing uncertainty analyses of WaTEM/SEDEM, it is important to consider sources of error  
490 associated to the RUSLE parameterisation. So far, uncertainty estimation methods applied to  
491 WaTEM/SEDEM have focused on the  $K_{TC}$  parameterisation, and therefore have underestimated the  
492 uncertainty in model predictions. We anticipate that our open-source WaTEM/SEDEM script will  
493 facilitate stochastic implementations of the model, and ultimately promote uncertainty and sensitivity  
494 analysis of soil erosion models. In particular, the open-source code will allow model users to explore

495 structural uncertainties, which can contribute to increase our understanding of sediment connectivity  
496 processes. As recent studies have again demonstrated, investigating the uncertainty in model  
497 structures, parameter estimation, and observational testing data is crucial for advancing soil erosion  
498 modelling research (Benaud et al., 2021; Eekhout et al., 2021; Schürz et al., 2020).

499 Importantly, while we demonstrated how conceptual models such as WaTEM/SEDEM can be useful  
500 for understanding structural connectivity patterns, more dynamic and process-oriented models are  
501 necessary for identifying so-called hot spots and hot moments of sediment connectivity (Owens, 2020;  
502 Turnbull and Wainwright, 2019). In addition, WaTEM/SEDEM representations of sediment transfer  
503 could be improved by incorporating the (dis)connectivity caused by linear features other than parcel  
504 borders and grass buffer strips. This might entail assimilating the  $P_{Con}$  parameter to features such as  
505 roadside ditches or terraces. Finally, mapping the location of hydraulic shortcuts within the road  
506 network, as well as the extent to which these shortcuts increase the connectivity from hillslopes to  
507 water courses (e.g., Schönenberger and Stamm, 2021), should further improve sediment connectivity  
508 simulations in areas such as the Baldegg catchment.

## 509 **5 Conclusions**

510 Here we employed a global sensitivity analysis of the WaTEM/SEDEM model to investigate the  
511 influence of linear structures and landscape patchiness on sediment connectivity in the Baldegg  
512 catchment. In particular, this novel application of WaTEM/SEDEM was implemented with the free  
513 programming language R, and our code is available as supplementary material.

514 Our results demonstrated that assumptions about road connectivity were by far the most important  
515 factor for modelling sediment transfer in the Baldegg catchment. Moreover, the comparison between  
516 extensive model simulations and sediment rating curve calculations indicated that roads and hydraulic  
517 shortcuts are likely to behave as conduits for sediment transport in the catchment. Hence, representing  
518 road connectivity is crucial for modelling sediment transfer from hillslope to water courses in this  
519 agricultural catchment of the Swiss Plateau, and potentially in other areas with a dense road drainage  
520 system. Moreover, our results further highlighted the effects of linear structures and landscape  
521 patchiness on sediment connectivity. These findings were made possible by the use of a model that  
522 was specifically tailored to explore the particularities of our study area, by effectively exploring model  
523 assumptions and the parameter space, and by the use of high resolution spatial data.

524 Overall, we found that WaTEM/SEDEM was useful for investigating sediment connectivity in the  
525 Baldegg catchment, as it allowed us to unravel some of the processes and structures regulating  
526 hillslope sediment transport in the area. In the case the model is used for prediction and decision-  
527 making, we recommend employing a fit-for-purpose rejectionist model testing framework, with  
528 multiple sources of data, in order to evaluate the model's numerical accuracy and the quality of its  
529 spatial predictions.

530 **6 Code availability**

531 The code for the model simulations was uploaded as a supplementary material file. If the manuscript is  
532 accepted, we will upload the R script file and input data used for the simulations to the EnviDat  
533 platform (<https://www.envidat.ch>).

534 **7 Data availability**

535 If the manuscript is accepted, we will upload the input data used for the simulations, and the raw  
536 sediment and discharge data to the EnviDat platform (<https://www.envidat.ch>).

537 **8 Author contributions**

538 PVGB and PF developed the model code, PVGB performed the simulations and analysed the data. SS  
539 prepared model input data. PVGB prepared the manuscript with contributions from all authors. CA  
540 was part of discussing ideas and revised the manuscript.

541 **9 Competing interests**

542 The authors declare no conflict of interest.

543 **10 Acknowledgements**

544 The authors would like to thank Robert Lovas, from the department of environment and energy of the  
545 Canton of Lucerne, for supplying the sediment concentration and water discharge monitoring data, and  
546 commenting on an earlier draft of this manuscript. We also appreciate the help from Axel Birkholz in  
547 acquiring the data. PVGB would like to thank Franz Conen and Claudia Mignani for their multiple and  
548 valuable inputs regarding the conceptualisation and preparation of this manuscript.

549

550 **References**

- 551 Alder, S., Prasuhn, V., Liniger, H., Herweg, K., Hurni, H., Candinas, A. and Gujer, H. U.: A high-  
552 resolution map of direct and indirect connectivity of erosion risk areas to surface waters in  
553 Switzerland-A risk assessment tool for planning and policy-making, *Land use policy*, 48, 236–249,  
554 doi:10.1016/j.landusepol.2015.06.001, 2015.
- 555 Antoniadis, A., Lambert-Lacroix, S. and Poggi, J. M.: Random forests for global sensitivity analysis:  
556 A selective review, *Reliab. Eng. Syst. Saf.*, 206, 107312, doi:10.1016/j.ress.2020.107312, 2021.
- 557 von Arb, C., Stoll, S., Frossard, E., Stamm, C. and Prasuhn, V.: The time it takes to reduce soil legacy  
558 phosphorus to a tolerable level for surface waters: What we learn from a case study in the catchment  
559 of Lake Baldegg, Switzerland, *Geoderma*, 403, doi:10.1016/j.geoderma.2021.115257, 2021.
- 560 Baartman, J. E. M., Nunes, J. P., Masselink, R., Darboux, F., Biielders, C., Degré, A., Cantreul, V.,  
561 Cerdan, O., Grangeon, T., Fiener, P., Wilken, F., Schindewolf, M. and Wainwright, J.: What do  
562 models tell us about water and sediment connectivity?, *Geomorphology*, 367, 107300,  
563 doi:10.1016/j.geomorph.2020.107300, 2020.
- 564 BAFU: Faktenblatt: Der Greifensee, Zustand bezüglich Wasserqualität, 1–8 [online] Available from:  
565 <http://www.bafu.admin.ch>, 2016.
- 566 Bakker, M. M., Govers, G., van Doorn, A., Quetier, F., Chouvardas, D. and Rounsevell, M.: The  
567 response of soil erosion and sediment export to land-use change in four areas of Europe: The  
568 importance of landscape pattern, *Geomorphology*, 98(3–4), 213–226,  
569 doi:10.1016/j.geomorph.2006.12.027, 2008.
- 570 Batista, P. V. G., Laceby, J. P., Davies, J., Carvalho, T. S., Tassinari, D., Silva, M. L. N., Curi, N. and  
571 Quinton, J. N.: A framework for testing large-scale distributed soil erosion and sediment delivery  
572 models : Dealing with uncertainty in models and the observational data, *Environ. Model. Softw.*, 137,  
573 doi:10.1016/j.envsoft.2021.104961, 2021.
- 574 Bauer, M., Dostal, T., Krasa, J., Jachymova, B., David, V., Devaty, J., Strouhal, L. and Rosendorf, P.:  
575 Risk to residents, infrastructure, and water bodies from flash floods and sediment transport, *Environ.*  
576 *Monit. Assess.*, 191(2), doi:10.1007/s10661-019-7216-7, 2019.
- 577 Benaud, P., Anderson, K., Evans, M., Farrow, L., Glendell, M., James, M. R., Quine, T. A., Quinton,  
578 J. N., Rickson, R. J. and Brazier, R. E.: Reproducibility, open science and progression in soil erosion  
579 research. A reply to “Response to ‘National-scale geodata describe widespread accelerated soil  
580 erosion’ Benaud et al. (2020) *Geoderma* 271, 114378” by Evans and Boardman (2021), *Geoderma*,  
581 402, doi:10.1016/j.geoderma.2021.115181, 2021.

582 Bircher, P., Liniger, H. and Prasuhn, V.: Aktualisierung und Optimierung der Erosionsrisikokarte (   
583 ERK2 ) Die neue ERK2 ( 2019 ) für das Ackerland der Schweiz, 2019.

584 Bispo, D. F. A., Batista, P.V.G., Guimarães, D. V., Silva, M. L. N., Curi, N. and Quinton, J. N.:   
585 Monitoring land use impacts on sediment production : a case study of the pilot catchment from the   
586 Brazilian program of payment for environmental services, *Rev. Bras. Ciência do Solo*, 44, :e0190167,   
587 2020.

588 Boardman, J.: A 38-year record of muddy flooding at Breaky Bottom: Learning from a detailed case   
589 study, *Catena*, 189(January), 104493, doi:10.1016/j.catena.2020.104493, 2020.

590 Borselli, L., Cassi, P. and Torri, D.: Prolegomena to sediment and flow connectivity in the landscape:   
591 A GIS and field numerical assessment, *Catena*, 75(3), 268–277, doi:10.1016/j.catena.2008.07.006,   
592 2008.

593 Breiman, L.: Random forests, *Machine Learning*, 45, 5-32, 2001.

594 Brenning, A., Bangs, D., Becker, M.: RSAGA: SAGA geoprocessing and terrain analysis. R package   
595 version 1.3.0., 2018.

596 Calsamiglia, A., García-Comendador, J., Fortesa, J., López-Tarazón, J. A., Crema, S., Cavalli, M.,   
597 Calvo-Cases, A. and Estrany, J.: Effects of agricultural drainage systems on sediment connectivity in a   
598 small Mediterranean lowland catchment, *Geomorphology*, 318, 162–171,   
599 doi:10.1016/j.geomorph.2018.06.011, 2018a.

600 Calsamiglia, A., Fortesa, J., García-Comendador, J., Lucas-Borja, M. E., Calvo-Cases, A. and Estrany,   
601 J.: Spatial patterns of sediment connectivity in terraced lands: Anthropogenic controls of catchment   
602 sensitivity, *L. Degrad. Dev.*, 29(4), 1198–1210, doi:10.1002/ldr.2840, 2018b.

603 Cavalli, M., Trevisani, S., Comiti, F. and Marchi, L.: Geomorphometric assessment of spatial   
604 sediment connectivity in small Alpine catchments, *Geomorphology*, 188, 31–41,   
605 doi:10.1016/j.geomorph.2012.05.007, 2013.

606 Chartin, C., Evrard, O., Salvador-Blanes, S., Hirschberger, F., Van Oost, K., Lefèvre, I., Daroussin, J.   
607 and Macaire, J. J.: Quantifying and modelling the impact of land consolidation and field borders on   
608 soil redistribution in agricultural landscapes (1954-2009), *Catena*, 110, 184–195,   
609 doi:10.1016/j.catena.2013.06.006, 2013.

610 Conrad, O., Bechtel, B., Bock, M., Dietrich, H., Fischer, E., Gerlitz, L., Wehberg, J., Wichmann, V.   
611 and Böhner, J.: System for Automated Geoscientific Analyses ( SAGA ) v.2.2.2, 1991–2007,   
612 doi:10.5194/gmd-8-1991-2015, 2015.

613 Croke, J., Mockler, S., Fogarty, P. and Takken, I.: Sediment concentration changes in runoff pathways  
614 from a forest road network and the resultant spatial pattern of catchment connectivity,  
615 *Geomorphology*, 68(3–4), 257–268, doi:10.1016/j.geomorph.2004.11.020, 2005.

616 Desmet, P., Govers, G.: A GIS procedure for automatically calculating the USLE LS factor on  
617 topographically complex landscape units, *J. Soil Water Conserv.*, 51, 427–433, 1996.

618 Eekhout, J. P. C., Millares-Valenzuela, A., Martínez-Salvador, A., García-Lorenzo, R., Pérez-Cutillas,  
619 P., Conesa-García, C. and de Vente, J.: A process-based soil erosion model ensemble to assess model  
620 uncertainty in climate-change impact assessments, *L. Degrad. Dev.*, 32, 2409–2422,  
621 doi:10.1002/ldr.3920, 2021.

622 Evrard, O., Cerdan, O., van Wesemael, B., Chauvet, M., Le Bissonnais, Y., Raclot, D., Vandaele, K.,  
623 Andrieux, P. and Bielders, C.: Reliability of an expert-based runoff and erosion model: Application of  
624 STREAM to different environments, *Catena*, 78(2), 129–141, doi:10.1016/j.catena.2009.03.009, 2009.

625 Fiener, P. and Auerswald, K.: Measurement and modeling of concentrated runoff in grassed  
626 waterways, *J. Hydrol.*, 301(1–4), 198–215, doi:10.1016/j.jhydrol.2004.06.030, 2005.

627 Fiener, P., Auerswald, K. and Van Oost, K.: Spatio-temporal patterns in land use and management  
628 affecting surface runoff response of agricultural catchments-A review, *Earth-Science Rev.*, 106(1–2),  
629 92–104, doi:10.1016/j.earscirev.2011.01.004, 2011.

630 Fiener, P., Wilken, F. and Auerswald, K.: Filling the gap between plot and landscape scale – eight  
631 years of soil erosion monitoring in 14 adjacent watersheds under soil conservation at Scheyern,  
632 Southern Germany, *Adv. Geosci. Discuss.*, (July), doi:adgeo-2019-4, 2019.

633 Fryirs, K.: (Dis)Connectivity in catchment sediment cascades: A fresh look at the sediment delivery  
634 problem, *Earth Surf. Process. Landforms*, 38(1), 30–46, doi:10.1002/esp.3242, 2013.

635 Gelman, A. and Hill, J.: *Data Analysis Using Regression and Multilevel/Hierarchical Models*,  
636 Cambridge University Press, New York., 2007.

637 Govers, G.: Misapplications and misconceptions of erosion models, in: *Handbook of erosion*  
638 *modelling*, edited by: Morgan, R. P. C., Nearing, M.A., Blackwell Publishing Ltd., Chichester, United  
639 Kingdom, 117–134, 2011.

640 Heckmann, T., Cavalli, M., Cerdan, O., Foerster, S., Javaux, M., Lode, E., Smetanová, A., Vericat, D.  
641 and Brardinoni, F.: Indices of sediment connectivity: opportunities, challenges and limitations, *Earth-*  
642 *Science Rev.*, 187(December 2017), 77–108, doi:10.1016/j.earscirev.2018.08.004, 2018.

643 IUSS Working Group WRB. *World Reference Base for Soil Resources; IUSS Working Group WRB:*  
644 *Wageningen, The Netherlands, 2006; pp. 1–128.*

645 Keller, B.: Lake Lucerne and its spectacular landscape, in: *Landscapes and landforms of Switzerland*,  
646 edited by Reynard, E., Springer Nature Switzerland, Cham, Switzerland, 305-324, 2021.

647 Krasa, J., Dostal, T., Jachymova, B., Bauer, M. and Devaty, J.: Soil erosion as a source of sediment  
648 and phosphorus in rivers and reservoirs – Watershed analyses using WaTEM/SEDEM, *Environ. Res.*,  
649 171(January), 470–483, doi:10.1016/j.envres.2019.01.044, 2019.

650 Kupferschmied, P.: CP-Tool: Ein Programm zur Berechnung des Fruchtfolge- und  
651 Bewirtschaftungsfaktors (CP-Faktor) der Allgemeinen Bodenabtragungsgleichung (ABAG), 2019.

652 Laceby, J. P., Batista, P. V. G., Taube, N., Kruk, M. K., Chung, C., Evrard, O. and Orwin, J. F.:  
653 Tracing total and dissolved material in a western Canadian basin using quality control samples to  
654 guide the selection of fingerprinting parameters for modelling, *Catena*, 200(April 2020), 105095,  
655 doi:10.1016/j.catena.2020.105095, 2021.

656 Lacoste, M., Michot, D., Viaud, V., Evrard, O. and Walter, C.: Combining  $^{137}\text{Cs}$  measurements and a  
657 spatially distributed erosion model to assess soil redistribution in a hedgerow landscape in  
658 northwestern France (1960-2010), *Catena*, 119, 78–89, doi:10.1016/j.catena.2014.03.004, 2014.

659 Lavrieux, M., Birkholz, A., Meusburger, K., Wiesenberg, G. L. B., Gilli, A., Stamm, C. and Alewell,  
660 C.: Plants or bacteria? 130 years of mixed imprints in Lake Baldegg sediments (Switzerland), as  
661 revealed by compound-specific isotope analysis (CSIA) and biomarker analysis, *Biogeosciences*,  
662 16(10), 2131–2146, doi:10.5194/bg-16-2131-2019, 2019.

663 Ledermann, T., Herweg, K., Liniger, H. P., Schneider, F., Hurni, H. and Prasuhn, V.: Applying  
664 erosion damage mapping to assess and quantify off-site effects of soil erosion in Switzerland, *L.*  
665 *Degrad. Dev.*, 21, 353–366, 2010.

666 Liaw, A., Wiener, M.: Classification and regression by randomForest. *R News*, 2, 18–22, 2002.

667 Mahoney, D. T., Fox, J. F. and Al-Aamery, N.: Watershed erosion modeling using the probability of  
668 sediment connectivity in a gently rolling system, *J. Hydrol.*, 561(April), 862–883,  
669 doi:10.1016/j.jhydrol.2018.04.034, 2018.

670 Mahoney, D. T., Fox, J., Al-Aamery, N. and Clare, E.: Integrating connectivity theory within  
671 watershed modelling part I: Model formulation and investigating the timing of sediment connectivity,  
672 *Sci. Total Environ.*, 740, 140385, doi:10.1016/j.scitotenv.2020.140385, 2020a.

673 Mahoney, D. T., Fox, J., Al-Aamery, N. and Clare, E.: Integrating connectivity theory within  
674 watershed modelling part II: Application and evaluating structural and functional connectivity, *Sci.*  
675 *Total Environ.*, 740, 140386, doi:10.1016/j.scitotenv.2020.140386, 2020b.

676 MeteoSwiss. SwissMetNet Surface Weather Stations, Mosen MOA, 2010-2019 (Switzerland), 2021.

677 Müller, B., Gächter, R. and Wüest, A.: Accelerated water quality improvement during  
678 oligotrophication in peri-alpine lakes, *Environ. Sci. Technol.*, 48(12), 6671–6677,  
679 doi:10.1021/es4040304, 2014.

680 Notebaert, B., Vaes, B., Govers, G., Van Oost, K., Van Rompaey, A., and Verstraeten, G.: *WaTEM /*  
681 *SEDEM version 2006 Manual.*, 2006.

682 Nunes, J. P., Wainwright, J., Biielders, C. L., Darboux, F., Fiener, P., Finger, D. and Turnbull, L.:  
683 Better models are more effectively connected models, *Earth Surf. Process. Landforms*, 43(6), 1355–  
684 1360, doi:10.1002/esp.4323, 2018.

685 Owens, P. N.: Soil erosion and sediment dynamics in the Anthropocene: a review of human impacts  
686 during a period of rapid global environmental change, *J. Soils Sediments*, 20(12), 4115–4143,  
687 doi:10.1007/s11368-020-02815-9, 2020.

688 Parsons, A. J., Wainwright, J., Brazier, R. E. and Powell, D. M.: Is sediment delivery a fallacy? Reply,  
689 *Earth Surf. Process. Landforms*, 34(February), 155–161, doi:10.1002/esp, 2009.

690 Persichillo, M. G., Bordoni, M., Cavalli, M., Crema, S. and Meisina, C.: The role of human activities  
691 on sediment connectivity of shallow landslides, *Catena*, 160(August 2016), 261–274,  
692 doi:10.1016/j.catena.2017.09.025, 2018.

693 Pianosi, F., Beven, K., Freer, J., Hall, J. W., Rougier, J., Stephenson, D. B. and Wagener, T.:  
694 Sensitivity analysis of environmental models: A systematic review with practical workflow, *Environ.*  
695 *Model. Softw.*, 79, 214–232, doi:10.1016/j.envsoft.2016.02.008, 2016.

696 Pfiffner, O. A.: The structural landscapes of Central Switzerland, in: *Landscapes and landforms of*  
697 *Switzerland*, edited by Reynard, E., Springer Nature Switzerland, Cham, Switzerland, 159-172, 2021.

698 Prasuhn, V.: Twenty years of soil erosion on-farm measurement: annual variation, spatial distribution  
699 and the impact of conservation programmes for soil loss rates in Switzerland, *Earth Surf. Process.*  
700 *Landforms*, doi:10.1002/esp.4829, 2020.

701 Remund, D., Liebisch, F., Liniger, H. P., Heinimann, A. and Prasuhn, V.: The origin of sediment and  
702 particulate phosphorus inputs into water bodies in the Swiss Midlands – A twenty-year field study of  
703 soil erosion, *Catena*, 203(March), 105290, doi:10.1016/j.catena.2021.105290, 2021.

704 Renard, K., Foster, G. R., Weesies, G. A., McCool, D. K. and Yoder, D. C.: *Predicting Soil Erosion by*  
705 *Water: A Guide to Conservation Planning With the Revised Universal Soil Loss Equation (RUSLE)*,  
706 1997.

707 R Core Team. *R: A language for statistical computing.* R Foundation for Statistical Computing,  
708 Vienna, Austria. URL <https://www.R-project.org>, 2021.



709 Saggau, P., Kuhwald, M. and Duttmann, R.: Integrating soil compaction impacts of tramlines into soil  
710 erosion modelling: A field-scale approach, *Soil Syst.*, 3(3), 1–28, doi:10.3390/soilsystems3030051,  
711 2019.

712 Schmidt, S., Alewell, C., Panagos, P. and Meusburger, K.: Regionalization of monthly rainfall  
713 erosivity patterns in Switzerland, *Hydrol. Earth Syst. Sci.*, 20(10), 4359–4373, doi:10.5194/hess-20-  
714 4359-2016, 2016.

715 Schmidt, S., Ballabio, C., Alewell, C., Panagos, P. and Meusburger, K.: Filling the European blank  
716 spot—Swiss soil erodibility assessment with topsoil samples, *J. Plant Nutr. Soil Sci.*, 181(5), 737–748,  
717 doi:10.1002/jpln.201800128, 2018a.

718 Schmidt, S., Alewell, C. and Meusburger, K.: Mapping spatio-temporal dynamics of the cover and  
719 management factor (C-factor) for grasslands in Switzerland, *Remote Sens. Environ.*, 211(April), 89–  
720 104, doi:10.1016/j.rse.2018.04.008, 2018b.

721 Schönenberger, U. and Stamm, C.: Hydraulic shortcuts increase the connectivity of arable land areas  
722 to surface waters, *Hydrol. Earth Syst. Sci.*, 25(4), 1727–1746, doi:10.5194/hess-25-1727-2021, 2021.

723 Schürz, C., Mehdi, B., Kiesel, J., Schulz, K. and Herrnegger, M.: A systematic assessment of  
724 uncertainties in large-scale soil loss estimation from different representations of USLE input factors—a  
725 case study for Kenya and Uganda, *Hydrol. Earth Syst. Sci.*, 24(9), 4463–4489, doi:10.5194/hess-24-  
726 4463-2020, 2020.

727 Starkloff, T. and Stolte, J.: Applied comparison of the erosion risk models EROSION 3D and LISEM  
728 for a small catchment in Norway, *Catena*, 118, 154–167, doi:10.1016/j.catena.2014.02.004, 2014.

729 Stenfert Kroese, J., Batista, P. V. G., Jacobs, S. R., Breuer, L., Quinton, J. N. and Rufino, M. C.:  
730 Agricultural land is the main source of stream sediments after conversion of an African montane  
731 forest, *Sci. Rep.*, 10(1), 1–15, doi:10.1038/s41598-020-71924-9, 2020.

732 Stoll, S., Arb, C. von, Jorg, C., Kopp, S. and Prasuhn, V.: Evaluation der stark zur Phosphor-Belastung  
733 des Baldeggersees beitragenden Flächen., 2019.

734 Swisstopo. SwissALTI3D. Das hoch aufgelöste Terrainmodell der Schweiz, 2014a.

735 Swisstopo. Swissimage. Das digitale Farbborthophotomosaik der Schweiz. 2014b.

736 Swisstopo. SwissTLM3D. Das grossmassstäbliche Topografische Landschaftsmodell der Schweiz,  
737 2020.

738 Teranes, J. L. and Bernasconi, S. M.: Factors controlling  $\delta^{13}\text{C}$  values of sedimentary carbon in  
739 hypertrophic Baldeggersee, Switzerland, and implications for interpreting isotope excursions in lake  
740 sedimentary records, *Limnol. Oceanogr.*, 50(3), 914–922, doi:10.4319/lo.2005.50.3.0914, 2005.

741 Turnbull, L. and Wainwright, J.: From structure to function: Understanding shrub encroachment in  
742 drylands using hydrological and sediment connectivity, *Ecol. Indic.*, 98(November 2018), 608–618,  
743 doi:10.1016/j.ecolind.2018.11.039, 2019.

744 Van Oost, K., Govers, G. and Desmet, P. J. J.: Evaluating the effects of changes in landscape structure  
745 on soil erosion by water and tillage, *Landsc. Ecol.*, 15(6), 577–589, doi:10.1023/A:1008198215674,  
746 2000.

747 Van Rompaey, A., Verstraeten, G., Van Oost, K., Govers, G. and Poesen, J.: Modelling mean annual  
748 sediment yield using a distributed approach, *Earth Surf. Process. Landforms*, 26(11), 1221–1236,  
749 doi:10.1002/esp.275, 2001.

750 Verstraeten, G., Van Oost, K., Van Rompaey, A. J. J., Poesen, J. and Govers, G.: Evaluating an  
751 integrated approach to catchment management to reduce soil loss and sediment pollution through  
752 modelling, *Soil Use Manag.*, 18(4), 386–394, doi:10.1111/j.1475-2743.2002.tb00257.x, 2010.

753 Vigiak, O. and Bende-Michl, U.: Estimating bootstrap and Bayesian prediction intervals for  
754 constituent load rating curves, *Water Resour. Res.*, 49(12), 8565–8578, doi:10.1002/2013WR013559,  
755 2013.

756 Wainwright, J., Turnbull, L., Ibrahim, T. G., Lexartza-Artza, I., Thornton, S. F. and Brazier, R. E.:  
757 Linking environmental regimes, space and time: Interpretations of structural and functional  
758 connectivity, *Geomorphology*, 126(3–4), 387–404, doi:10.1016/j.geomorph.2010.07.027, 2011.

759 Wang, Y. G., Kuhnert, P. and Henderson, B.: Load estimation with uncertainties from opportunistic  
760 sampling data - A semiparametric approach, *J. Hydrol.*, 396(1–2), 148–157,  
761 doi:10.1016/j.jhydrol.2010.11.003, 2011.

762 Wehrli, B., Lotter, A. F., Schaller, T. and Sturm, M.: High-resolution varve studies in Baldeggersee  
763 (Switzerland): Project overview and limnological background data, *Aquat. Sci.*, 59(4), 285–294,  
764 doi:10.1007/BF02522359, 1997.

765 Wilken, F., Fiener, P. and Van Oost, K.: Modelling a century of soil redistribution processes and  
766 carbon delivery from small watersheds using a multi-class sediment transport model, *Earth Surf. Dyn.*,  
767 5, 113–124, doi:10.5194/esurf-5-113-2017, 2017.

768